Applied Energy 268 (2020) 114925

Contents lists available at ScienceDirect

Applied Energy

journal homepage: www.elsevier.com/locate/apenergy

Sandstorm erosion on solar reflectors: Highly realistic modeling of artificial aging tests based on advanced site assessment

F. Wiesinger[a,*], F. Sutter[a], A. Fernández-García[b], J. Wette[a], F. Wolfertstetter[a], N. Hanrieder[a], Martin Schmücker[c], R. Pitz-Paal[d]

[a] German Aerospace Center (DLR), Institute of Solar Research, Paseo de Almería, 73, 2, 04001 Almería, Spain
[b] Centro de Investigaciones Energéticas, Medioambientales y Tecnológicas (CIEMAT), Plataforma Solar de, Almería (PSA), Ctra. de Senés/n km 4, Apartado 22, 04200 Tabernas, Spain
[c] German Aerospace Center (DLR), Institute of Material Research, Linder Höhe, D-51147 Cologne, Germany
[d] German Aerospace Center (DLR), Institute of Solar Research, Linder Höhe, D-51147 Cologne, Germany

HIGHLIGHTS

- Outdoor exposure of CSP mirrors at 5 sites accompanied with meteo data acquisition.
- Assessment of 6 erosion determining factors for the different sites.
- Development of a novel image processing technique to characterize the mirrors.
- Modeling artificial aging experiments (AAE) to simulate realistic erosion effects.
- Definition of 3 erosion classes of outdoor sites & presentation of respective AAE.

ARTICLE INFO

Keywords:
Solar energy site assessment
CSP component qualification
Accelerated aging simulation
Sandstorm erosion
Solar reflector degradation

ABSTRACT

In this work a guideline is developed which allows for a highly realistic laboratory simulation of sandstorm effects on glass components for the solar industry. So far no standardized test procedure is developed to test components against each other and predict their lifetime in the field to a realistic extent. One important reason for that matter is the strong variation from one site to another which would have to be addressed in a standardized test procedure. To overcome this issue, the meteorological and geological parameters of five outdoor sites are investigated in this work regarding their erosion potential, and additionally state of the art silvered-glass reflector samples are exposed. A special focus is laid on the relative humidity, *rh*, and wind velocity, *u*, present at the same time (here named as *u-rh* couple). It is shown that strong winds accompanied with low relative humidity are more often measured at sites where the reflectors are more severely damaged by impacting sand particles. Apart from the *u-rh* analysis, the mineralogical characteristics of the sites are investigated and both the particle size distribution and the chemical composition of the soil are presented. In total, six erosion determining factors are identified and the five investigated sites are qualitatively ranked and sorted into three erosivity classes. The input parameters of a laboratory erosion setup were tailored in order to meet the conditions of the three erosivity classes. Therefore state of the art reflectance measurements are used, but also a novel method, based on image processing of microscope pictures of the mechanical defects on the glass surface is presented. This method enables the determination of a *defect size density distribution* (DSDD). The test parameters of the laboratory setup are adjusted in order to achieve a similar DSDD like observed outdoor for the three different erosivity classes.

1. Introduction & motivation

By the year 2040 > 20% of the global energy production is expected to be based on renewable sources [1]. Solar energy is going to be a major part of this share but the steady growth of this technology is coupled to the sophistication and the upscaling of system size. To ensure reliability, maintainability and safety of large scale projects at novel sites, the analysis of the main degradation mechanisms and

* Corresponding author.
E-mail address: florian.wiesinger@dlr.de (F. Wiesinger).

https://doi.org/10.1016/j.apenergy.2020.114925
Received 25 November 2019; Received in revised form 5 March 2020; Accepted 27 March 2020

Nomenclature

Acronyms

PSA	Plataforma Solar de Almería
CSP	concentrated solar power
PV	Photovoltaic
DSDD	defect size density distribution
PSD_{num}	particle size distribution (numerical)
SDS	sand- and dust storms
EDX	energy dispersive X-ray module
D&S	Devices and Services

Symbols

GHI	global horizontal irradiation [W m^{-2}]
DNI	direct normal irradiation [W m^{-2}]
DD	defect density [mm^{-2}]
TSP	total suspended particle concentration [μg m^{-3}]
u	wind velocity [m s^{-1}]
rh	relative humidity [%]
D_d	defect diameter [μm]
D_p	particle diameter [μm]
β	impact angle sand-reflector [°]
m_a	impacting sand mass per reflector area [g cm^{-2}]
ρ	reflectance [-]
α	absorptance [-]

respective techniques to prevent and mitigate these faults is inevitable.

High annual irradiation levels in the MENA-region attract an increasing number of solar energy plant developers. The high aridity in the respective areas leads to increased aerosol loads in the lower atmospheric layer close to the ground [2]. In the first place, this can significantly reduce optical efficiency of concentrated solar power (CSP) and photovoltaic (PV) plants due to soiling effects [3,4]. For central receiver systems (CRS), a second effect called atmospheric extinction [5] is an additional handicap. A third effect is windblown aerosol particles, which may cause material wear on the structures, and significant energy conversion efficiency losses, when impacting on surfaces of optical components like the absorbers or reflectors of solar power plants, reducing their optical absorptance, α, or their reflectance, ρ, respectively. All of the three effects lead to optical performance losses which decrease the economic benefit of solar power plants. In their review paper, Gonzalo et al. [6] mentioned these three critical effects to be of mayor concern for the future development of the solar energy technology. Soiling is reversible via cleaning, which mostly requires a combination of manpower, energy and water [7,8]. The other two, atmospheric extinction and sandstorm erosion, can be regarded as inevitable site specific phenomena that can hardly be avoided and their contribution to the overall efficiency loss should be minimized by a smart technology selection for the respective site. Measurement approaches which determine the temporal resolved onsite atmospheric extinction within different uncertainly limits and maintenance effort have been presented during the last years [9]. Additionally, a transmittance model which derives the atmospheric transmittance on potential sites in the MENA region for CRS systems has been developed [10] and validated [11]. The model derives the atmospheric transmittance between a heliostat and receiver on the basis of common direct normal irradiance (DNI), temperature, relative humidity and barometric pressure measurements.

A proper site assessment concerning the erosion danger of sand particle impacts on optical surfaces appears to be more difficult, because not only meteorological, but also geological parameters have to be taken into account. In an earlier work by the current group [12], the most important issues which point towards an increased risk of potentially hazardous sand- and dust movement were summarized as follows:

1. The particle size distribution of the soil material exhibits a maximum around 65–200 μm.
2. The particle size distribution is of a bimodal nature.
3. The terrain exhibits no surface features and is basically a vast plain without vegetation or obstacles serving as wind barrier. Wind velocities are often measured to be higher than 10 m s^{-1} (at 10 m above ground).
4. Low relative humidity *rh* and high wind velocities *u* are present at the same time.
5. High total suspended particle concentrations *TSP* (> 1000 μg m^{-3}) are measured.
6. Low clay content of the soil is present which leads to less efficient water adsorption which lowers the soil moisture and in the end favors saltation.
7. High quartz content of the soil is present which will lead to intensive erosion effects if particles reach saltation mode due to the hardness of quartz.

Not all the above mentioned points have to be fulfilled in order to deduce an increased erosion potential for the respective site but in general it can be stated that the more conditions are fulfilled the higher the risk.

It shall be pointed to the fact, that an underestimation or complete disregard of reflectance losses due to erosion can lead to major consequences for the plant performance, since the generated damages are permanent and are accumulating over time. Marginally appearing reflectance losses of 1% will result in an annual economic loss of 0.75 Mio $ for a 50 MW CSP plant in southern Spain [13]. Even though the here presented work focuses on reflectors for CSP applications, the obtained results are valuable for PV panels or flat plate collectors as well. In general, materials have to be chosen so that their durability meets the demands, corresponding to a 20 to 25 yearlong outdoor exposure under certain environmental impacts [14]. In order to qualify the materials for such conditions, accelerated aging tests are conducted. These are standard procedures which are widely applied already and reproduce the effects caused by e.g. marine environments (salt spray test according to ISO 9227), long-term UV-radiation and cyclic condensation (ISO 16474-3) or by thermal cycles (IEC 61215). There is a strong interest of the CSP and the PV industry to develop a testing standard which is capable of estimating the lifetime of optical components under sandstorm conditions, and many different groups recently developed accelerated erosion setups for this purpose. For example Sansom et al. [15] operated a pressurized sandblasting setup were two different sands from Libya and an artificial one were used to simulate four hour lasting sandstorms. An open circuit sand blower machine was used by Karim et al. [16] and natural as well as artificial sand samples were facilitated to determine the influence of several parameters on the erosion effects. In their study Humood et al. [17] also used an air compressor and a blast gun with a nozzle to investigate the normal impact of artificial silica sand on solite glass. Matal et al. [18] used a test bench which also works with pressurized air to assess the performance of an anti-soiling coating. Völker et al. [19] and Wiesinger et al. [20] performed investigations with a vertical soil pipe were sand is falling on different reflector types only accelerated by gravity. Furthermore Wiesinger et al.

[21] facilitated a closed loop wind tunnel to investigate different anti-reflective coatings for solar glass. So far, there is no realistic standard erosion test available to simulate erosion effects on optical components caused by sand- and duststorms (SDS). The MIL-STD-810G as well as ASTM-D968-05 and DIN 52348 are not considered as meaningful in this context since they are too aggressive and consequently the damages caused on the materials are of inadmissible nature [22,23].

As it is stated in Gonzalo et al. [6], not enough studies about erosion mitigation are available and the current authors think that the reason for that is both an incomplete understanding of the natural processes leading to the respective effect and a lack of laboratory guidelines to simulate the realistic erosion under controlled conditions in order to arrive at reasonable mitigation techniques.

The objective of the current work is on one hand, to proof the validity of an earlier developed site assessment checklist concerning potential sand erosion danger for three additional sites. Furthermore, item number four on the checklist (dealing with the presence of low *rh* during high *u* events) was upgraded from a qualitative to a quantitative basis, since now the absolute hours, where certain *u*-*rh* couples present favorable saltation conditions, are evaluated. The points from the checklist are rated for the investigated sites and by that an erosion potential matrix is developed where ambient conditions are given in terms of their relevance for erosion processes. This matrix shall be of interest for plant developers in order to ensure the long-term energy conversion efficiency of the employed optical parts of the plant. It shall be further referred to the work of Pescheux et al. [24], who did a similar site assessment work especially focused on the sand characteristics at five Moroccan sites.

On the other hand, a novel damage characterization technique is introduced which is based on microscope image processing. This innovative tool facilitates the exact reproduction of the defect picture of the outdoor exposed reflectors under laboratory conditions. In the following, this technique is used to model the accelerated aging tests results and develop a guideline which shall be applied to new reflector materials when they are to be tested to simulate long outdoor exposure at distinct environmental areas. It can be summarized as a highly specialized approach to simulate the erosion defects on reflectors for solar energy to such a realistic extent, never reached before in this field. Based on the erosion severeness from the outdoor exposed reflectors three erosivity classes are defined which can be used as input parameters for lifetime prediction calculations.

2. Methodology

This section describes the environmental conditions of the five outdoor sites where sample exposure took place. Afterwards an introduction on reflector quality assessment is given and the developed image processing technique is explained in detail. Furthermore the laboratory erosion setup is presented.

2.1. Description of the outdoor sites

For this study, results from a 1 year outdoor exposure campaign in **Missour** (32°, 51′ N; 4°, 6′ W), **Erfoud** (31°, 29′ N; 4°, 13′ W), **Zagora** (30°, 16′ N; 5°, 51′ W) (all three in Morocco), **Tabernas (PSA)**, Spain (37°, 6′, N; 2°, 21′ W) and **Chajnantor**, Chile (23°, 05′ S; 67° 40′ W) are used. The sites are abbreviated by: MIS, ERF, ZAG, PSA and CHA, respectively. Apart from CHA, the stations belong to the enerMENA meteorological network [25,26] and are selected for this study because they are representative sites for CSP plant locations. Chajnantor is selected since currently Chile is a fashion place for the CSP industry and because of its extremely high solar irradiation level. The general meteorological data of CHA is downloaded from the SoDa Web site [27]. The exposure time was from January 2017 to January 2018 for MIS, ERF and ZAG and from March 2017 until March 2018 for PSA and CHA. All the sites can be described as arid zones with poor vegetation and exhibit high direct normal- and global horizontal irradiation values which make the sites suitable for CSP and PV applications. An overview of the general meteorological data is given in Table 1. The meteorological data is evaluated in the same timeframe as the exposure data of the reflectors. The given *u* and *rh*, are 1-minute average values. *u* is measured at 10 m above ground. The overall data completeness is 89.6, 97.2, 86.9, 96.5 and 97.0% for MIS, ERF, ZAG, PSA and CHA, respectively.

Table 1
Annual mean of meteorological data.

Site	MIS	ERF	ZAG	PSA	CHA
Temperature [°C]	18.0	22.2	23,9	18.3	5.4
Relative humidity, *rh* [%]	48.1	30.1	23.4	59.5	26.1
Wind velocity, *u* [m/s]	3.6	3.1	3.8	3.2	4.1
Hours of $u > 10$ [h]	227	42	221	85	339
GHI [kWh/m^2]	2023	2044	2174	1901	–

Meteorological data acquisition is accompanied with the exposure of state of the art second-surface silvered-glass reflectors for CSP applications. The exposed samples have spatial dimensions of (10 × 10) cm^2 with a 2 mm thickness and are facing south (180°) (in case of CHA north (0°)) under a horizontal elevation angle of 45° at an approximate height of (1.2 ± 0.2) m above ground, depending on the exact position on the rack (see Fig. 1).

In order to characterize the sand particles present at the sites, soil samples are manually taken from the topsoil layer from the ground. On the one hand, they are analyzed via an optical microscope Axio CSM 700 from Zeiss (Oberkochen, Germany) to determine the numerical size distribution PSD_{num} which shows the number of particles in a certain particle diameter (D_p)-range (see section 2.2). On the other hand, an electron microscope type Gemini Ultra 55, manufactured by Zeiss (Oberkochen, Germany) with an INCA FETx3 energy dispersive X-ray module (EDX) is used to determine the elemental composition.

Since local surface morphology plays a crucial rule for the saltation potential, it is described here in short for the various sites of this campaign. The location in MIS is situated in a low hilly area with some surface features which generally represent minor wind obstacles. There are a few low buildings in a circumference of around 200 m and the vegetation consists of low shrubs. For ERF the situation is quite similar, the station lies in the outskirts of a large hotel complex, around 100 m away from buildings or larger palm trees. In the near vicinity there are only some 0.5 m high, young palm trees and a fence along the southwestern edge of the station. The ZAG site can be explained as a vast open plain with no surface features at all, low shrubs are sparsely distributed around the area. The PSA site exhibits various surface features in the close vicinity of the reflector rack; a heliostat field and a parabolic-trough collector loop are located to the south and the west of the reflector rack, respectively.

The CHA exposure site is located in a high-altitude area of the Atacama desert (5200 m above sea level). It is characterized by its lack of vegetation and rocky ground. Several one-story buildings and containers are located in a radius of ca. 100 m. Surface morphology and natural or man-made wind obstacles are determinants for the evolution of strong winds ($u > 10$ m/s). The absolute hours where these high wind events are measured over the course of the exposure time are also given in Table 1.

2.2. Reflector qualification and image analysis

Concerning the quality assessment of solar mirrors, the reflectance is the most common parameter. Reflectance values depend on the measurement parameters: incident angle, wavelength and acceptance angle, denoted as θ, λ and φ, respectively. State of the art second-surface silvered-glass reflectors can achieve a monochromatic specular reflectance $\rho_{\lambda,\varphi}$ of > 0.965 for $\theta = 15°$, $\lambda = 660$ nm and

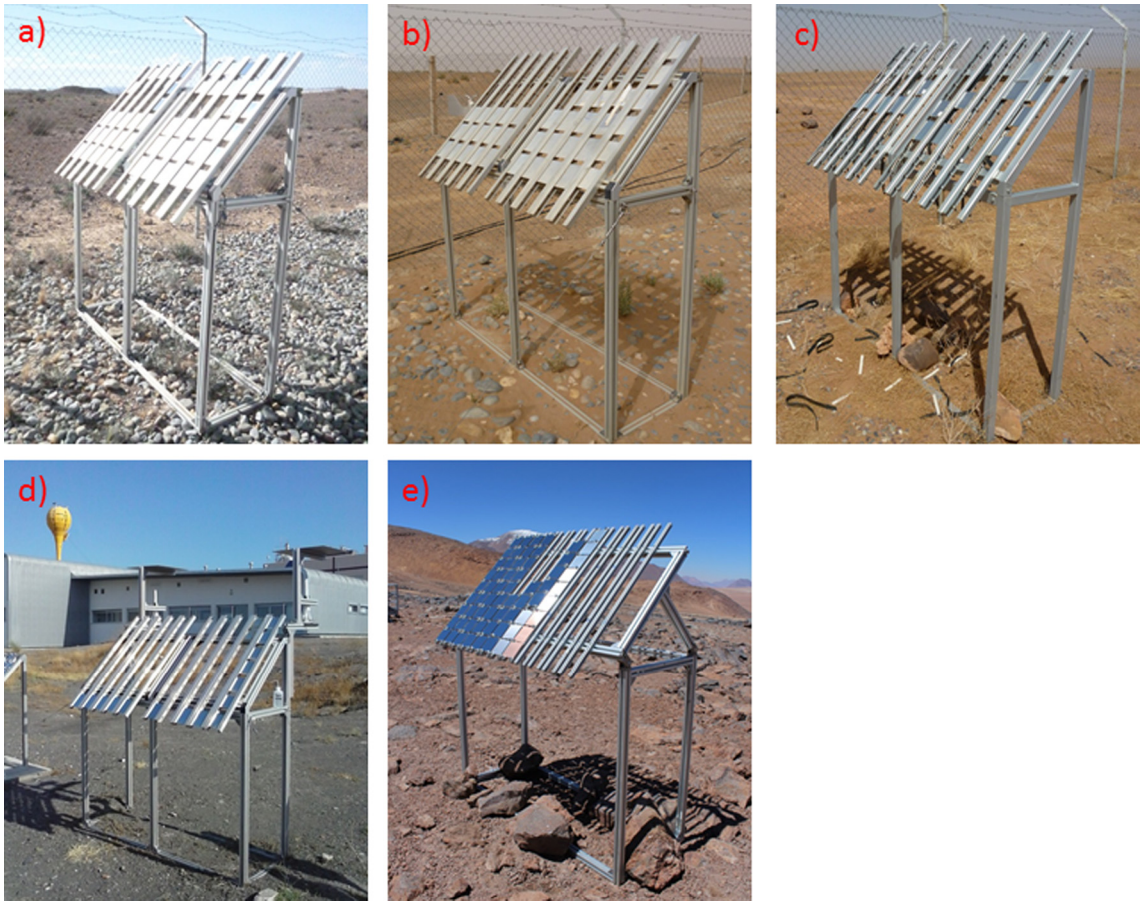

Fig. 1. Rack structure for the exposure of reflector samples in a) Missour, b) Erfoud, c) Zagora, d) PSA and e) Chajnantor.

φ = 12.5mrad. For the $\rho_{\lambda,\varphi}$ measurements with these parameters, the D&S 15R-USB (hereafter: D&S) from Devices and Services (Dallas/USA) is often used. The uncertainty of the equipment is 0.003. The measurement spot of the D&S on the tested specimen exhibits a diameter of 1 cm, hence no spatial resolved measurements can be conducted, which is of minor interest for new and homogeneous reflector materials. For inhomogeneous reflectors, or reflectors which are soiled or damaged during artificial or natural aging experiments, multiple D&S measurements shall be conducted and the average value together with its standard deviation shall be reported [28].

One has to keep in mind, that artificial aging experiments leading to a similar monochromatic specular reflectance loss $\Delta\rho_{\lambda,\varphi}$ are no proof of the correct simulation of the natural failure mechanism. The reasons leading to the measured $\Delta\rho_{\lambda,\varphi}$ could be of versatile nature. In earlier studies dealing with artificial erosion experiments to simulate the effects of sandstorms on second-surface silvered-glass reflectors, it could be concluded that the realistic reproduction of the effects caused under natural circumstances is of crucial importance in order to make

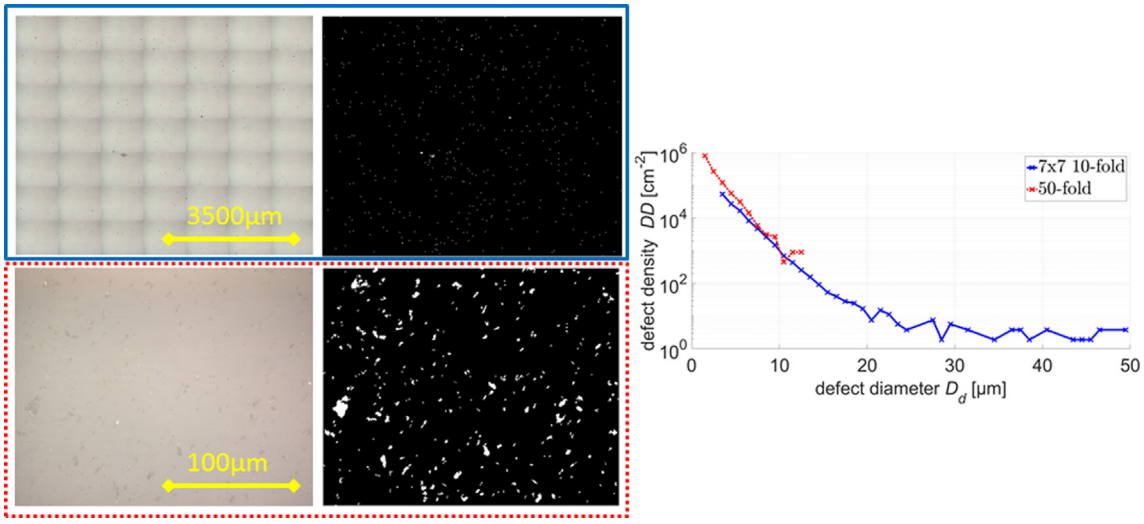

Fig. 2. Illustration of the working principle of the defect detection on a 7x7 10-fold, and one 50-fold microscope image with their resulting DSDD.

predictions over the long term behavior of the respective materials. It was especially pointed to the fact that the employed artificial aging simulation was not able to reproduce small defects, which were observed on the outdoor exposed reflectors and are expected to contribute to $\Delta\rho_{\lambda,\varphi}$ [20].

In the here presented work, a novel image analysis technique is used in addition to the D&S measurements in order to verify the accurate simulation of the artificial erosion experiment. This technique is based on the evaluation of images of the defects on the glass surface taken by microscope. The procedure is illustrated in Fig. 2. The image acquisition process takes place using a 10-fold magnification objective and the so-called patchwork mode of the microscope software. Multiple adjacent images (in this case 7x7) are taken and stitched together to compose a total area of around 0.5 cm^2. Thereby, a high magnification of a large area is achieved. For image analysis, the image processing toolbox of Matlab is used. A so-called *flatfield image* is taken at the same illumination and magnification conditions of the surface of a new reflector sample of the same type. By the application of a flatfield image subtraction, the uneven illumination pattern which is seen in Fig. 2 can be removed. In the next steps, conversion to grey values, brightness thresholding and a binary conversion takes place. The resulting objects are separated in size classes of 1 μm width, ranging from 1 μm to 50 μm and the quantity in each of the bins is given as density with respect to the evaluated reflector area. This leads to a defect size density distribution (DSDD), which is considered to be characteristic for erosion processes of particular environments.

The spatial dimension of one pixel in a 10-fold magnification image is around 1 μm, but due to noise reduction and to avoid falsely detected defects, this theoretical resolution is never reached. However it is noticed that e.g. in the case of ZAG many defects are in this particular size range. An exclusive usage of the next higher magnification objective (50-fold) would not allow for a large area to be investigated without extensive production of data and would be time intensive, since the patchwork scan of 35 × 35 picture (same spatial dimensions as with 10-fold 7 × 7) is not feasible for this kind of investigation. To overcome this issue, the results from ten randomly taken 50-fold magnified areas are combined with the 7 × 7 10-fold images. The two resulting DSDD are overlapping in a certain D_d-area. As seen in Fig. 2 (right), the DSDD determined by both methods coincide, validating the applied methodology.

In order to perform realistic erosion experiments under accelerated conditions in the laboratory, the DSDD of the outdoor exposed reflector materials are obtained and afterwards reproduced on new reflectors in an in-house developed accelerated aging chamber [29].

A similar method like the defect detection is applied to investigate soil samples from the different sites and obtain a particle size distribution (PSD_{num}). To this end, the as-collected sand is mechanically sieved (mesh aperture 425 μm) and around 50,000 particles which pass the sieve are optically analyzed.

2.3. Artificial sand erosion chamber

In order to conduct accelerated erosion experiments, an open-loop wind tunnel with particle injection –named Acetube- was constructed at the PSA [29]. A sketch of its working principle is given in Fig. 3. The specimen to be tested is mounted in the transparent box on a rotating plate to establish a homogeneous defect distribution over the sample surface [30]. The impact angle β is fixed at 45° to meet the conditions of the outdoor setup (see section 2.1). The dependence of erosion effects on β is widely investigated for comparable situations and it should not be addressed in the here presented work (see e.g. [31–33]). To calibrate the wind velocity in reference to the axial ventilator power, the sample holder is exchanged for an ultrasonic wind sensor from FT technologies Ltd. The wind velocity for the erosion testing is chosen to be 20 m/s. This velocity was eventually present at all sites and can be regarded as a representative worst-case testing scenario. For the interested reader who wants to know more about the details on velocity dependence of sand particles on glass erosion for solar applications, it may be referred to [31]. In order to fulfill the requirement of reproducible erosion results and to ensure that other laboratories can perform similar testing, two commercially purchased artificial erodent materials are used: MIL-STD-810 blowing dust (hereafter: MIL-dust) and MIL-STD-810 blowing sand (hereafter: MIL-sand). Both were obtained from KSL (Lauingen, Germany) and are composed mainly out of quartz (97–99% and ≥95% for MIL-dust and MIL-sand, respectively). The MIL-dust has fine particles with a diameter range lying between < 1 and 150 μm while the MIL-sand is more coarse and exhibits a particle diameter distribution between 149 and 850 μm.

The properties of this particular accelerated erosion simulation setup lead to significant advantages over the closed loop or pressurized air gun setups, which have been used in other studies like Caron [34], Bouaouadja et al. [35] or Karim et al. [16]. In contrast to the closed loop setup, the erosion particle characteristics are not altered by repeated impacts on the tube walls before they reach the specimen, neither are inadvertent metal particles, caused by wear of the inner tube walls, involved in the erosion process. Furthermore, the amount of particles affecting the surface is very well determined by the adjustment of the inserted particle mass. The specimen tested in the Acetube does not exhibit an inhomogeneous erosion picture, in contrast to many pressurized air gun setups which produce a central spot of more intensive erosion which decreases radially to outer parts of the specimen. On the one hand, this is avoided by rotating the sample and on the other hand, by a tube diameter which is larger than the specimen dimensions. By referring the inserted sand mass to the cross section area of the tube (diameter of 20 cm) the impacting sand mass per reflector area, m_a, in g cm^{-2} can be calculated. The application of an area related impact mass is of crucial importance to guarantee the comparability of different erosion simulation setups.

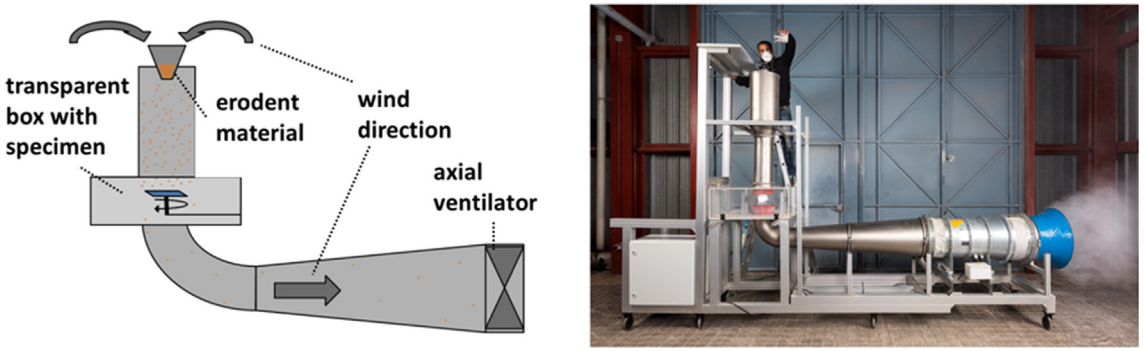

Fig. 3. Acetube Setup at PSA (sketch on the left and real life on the right).

3. Results & discussion

The following section is divided into two subsections. In the first one, the results of the outdoor measurements are presented and used to develop an erosion potential matrix. This matrix can be consulted as a first reference, when the suitability of a site for CSP technologies shall be assessed. Furthermore, the analysis of the exposed reflector samples is presented, which substantiates the statements in the erosion matrix.

The second section deals with the results of the accelerated erosion simulation in the laboratory and its comparison to the real outdoor effects. A procedure is developed, that allows to reproduce DSDD within accelerated erosion tests on optical components, allowing to simulate exposure at each of the 5 outdoor sites in a very short time frame (in the magnitude of a couple of minutes).

3.1. Outdoor data analysis

The first subsection presents the results from the analysis of the soil samples taken from the various sites, namely the obtained PSD_{num} and the mineralogical composition. Afterwards, the meteorological data dealing with a profound analysis of the *u-rh* couples is presented for Missour, Erfoud, Zagora and the PSA; Chajnantor was left out because data was of insufficient quality for a meaningful comparison. Thereafter, the aging effects of the outdoor exposed reflectors are quantified. The main results from this subsection are summarized in an erosion potential matrix.

3.1.1. Soil analysis

Soil samples from the five different sites are investigated via an image analysis procedure, and the resulting PSD_{num} are shown in Fig. 4. The as-collected sand from the sites is mechanically sieved (mesh aperture 425 µm) and a few thousand particles which passed the sieve are optically analyzed. The amount N of particles with a certain diameter D_p is sorted in size bins of 5 µm resolution ranging from 1 to 500 µm. The ratio of the particles smaller than 10 µm is 93.5, 97.7, 86.7, 93.0 and 95.4% for Missour, Erfoud, Zagora, PSA and Chajnantor, respectively. It can be seen that the PSD_{num} is decreasing monotonously towards higher diameters for Missour. For the PSA, one can observe a plateau region of the PSD_{num} which starts at a D_p of around 30 µm. For the sand samples from Erfoud and Chajnantor there is a local maximum in the PSD_{num} detectable at roughly 60 µm. This maximum becomes even more pronounced for the sand from Zagora. It is known from many wind tunnel experiments that the threshold friction velocity, which corresponds to the particular wind speed, which is necessary to lift particles from the ground and bring them in saltation mode, takes on a minimum for particles of a certain diameter. A parent bed of similar, equally sized and uniform soil particles was used in the calculations of Darmenova et al. [36] and it could be concluded, that for small particles the inter-particle cohesive forces, and for larger particles their gravitational force, impede particles from leaving the bed. However, for particles in the size range around 65 to 200 µm, a minimum for the threshold friction velocity could be determined [37–39]. Hence it can be assumed, that the presence of here detected second mode of the PSD_{num} (the first mode is located in the submicron range) and its overlap with the minimum of the threshold friction velocity favors the onset of saltation at site in Erfoud, Chajnantor and especially in Zagora.

Table 2
Results from EDX-analysis of soil samples taken at the different sites chemical composition values taken from the datasheets of the respective artificial sands given as mass fraction [wt%].

	Na_2O	K_2O	MgO	Al_2O_3	SiO_2	CaO	Fe_2O_3	SO_2
Missour	1	1	–	4	13	67	–	14
Erfoud	–	1	1	3	59	33	3	–
Zagora	1	3	1	8	73	8	5	1
PSA	1	4	1	18	66	2	8	–
Chajnantor	3	3	1	16	69	4	4	–
MIL-dust					97–99			
MIL-sand					> 95			

Elemental analysis and the conversion to the most prominent oxide compounds lead to the mineralogical composition in Table 2. With exception of the soil from Missour, the major constituent of the soil is quartz followed by some minor percentages of clay- and carbonate minerals. The situation is different for the soil from Missour where quartz is only contributing around 13 wt% to the total mass. More than two thirds of the soil in Missour are carbonate minerals and around 14 wt% of gypsum could be identified. When taking into account the hardness values of the most present minerals (i.e. from Stachowiak and Batchelor 2013 [32]), one can conclude that the erosion potential of the soil from Missour is significantly lower than the soil from the other sites. Artificial erosion experiments conducted in an earlier study by the current group [12], where soil from Missour and Zagora was employed, supports this thesis as well.

High clay content, leads to augmented water absorption capacity. Therefore, a higher mean soil moisture is expected [40], which impedes saltation. A simple experiment is conducted to provide further evidence

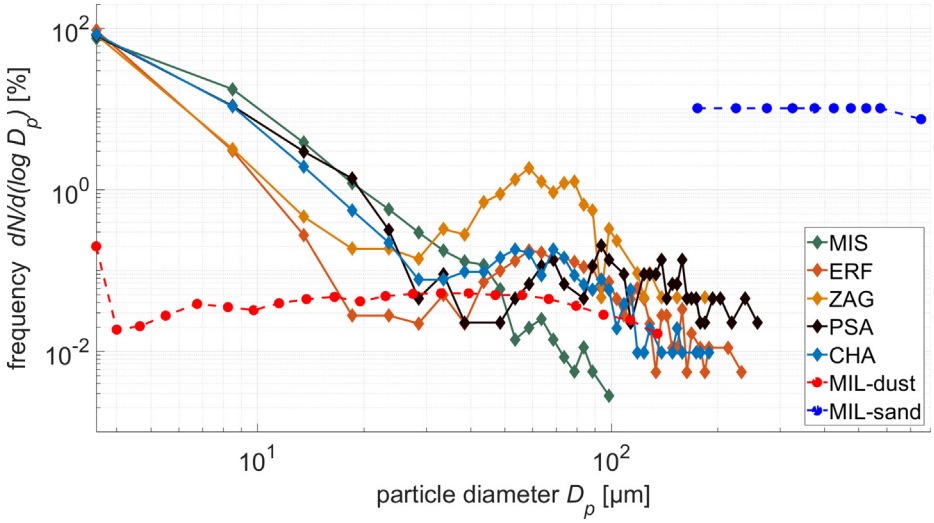

Fig. 4. PSD_{num} of soil fractions < 425 µm from Missour, Erfoud, Zagora, PSA and Chajnantor, evaluated via optical microscopy. PSD_{num} of the two artificial dusts are extracted from the datasheets.

on the water adsorption potential of the soils from the different sites. A small sample of the respective soils is exposed overnight outdoor at the PSA at a relative humidity around 50%. In the morning the samples are weighed and then heated up to 80° for two hours to remove the adsorbed water. Immediately afterwards, the samples are weighed again and the relative mass loss is derived. The relative mass losses for the soil from Missour, Erfoud, Zagora, PSA and Chajnantor are calculated to 0.3%, 0.05%, 0.08%, 0.08% and 0.08%, respectively. From this experiment it becomes clear, that under the natural conditions, present during the adsorption process, the soil of Missour has a water adsorption potential which is between 3.8 and 6 times higher than for the soils from the other sites. Assuming similar relative air humidity, soils like present in Missour are supposed to exhibit higher soil humidity throughout the year and are therefore less susceptible for erosion.

3.1.2. Evaluation of u-rh couples

Some general meteorological data are shown in Table 1 already and are analyzed more thoroughly in this section. In order to lift particles up from the ground, low soil humidity and high wind velocities are favorable [12,36]. Even though the soil humidity is not known for this study, *rh* was taken as a parameter that in general correlates to soil humidity in arid regions [41]. From average values of both parameters over long periods of time like in Table 1 no accurate conclusions can be made about the frequency and duration of events, where both parameters are in a favorable range to promote saltation. To overcome this issue, Fig. 5 shows a histogram presenting the occurrence of certain *u-rh* couples in a color scale for Missour, Erfoud, Zagora and the PSA. The resolution is 1 m s^{-1} and 5%, for *u* and *rh*, respectively. Only *u-rh* couples are taken into account where the wind direction was 180° (± 90°) since the exposed reflector samples are facing south. Unfortunately the data from Chajnantor was of insufficient quality and quantity to perform such an evaluation.

From this graph, it can be noted that the PSA site behaves different than the remaining three sites. Most of the time *u* values between 1 and 3 m/s are measured which are accompanied by an *rh* between 25 and 90%. This is also the case for MIS although there is also a significant contribution of *u-rh* couples which are representing strong winds at dry conditions. In ERF and ZAG the most frequent *u-rh* couples are found at dry conditions of < 40% and 25% humidity, respectively. It should be mentioned, that there is no discrete limit for neither *u* nor for *rh* from which the onset of saltation can be regarded to take place at a higher efficiency, furthermore there are various cross-dependencies to other physical parameters i.e. the particle size distribution of the soil, the clay content, the roughness length, etc. [36]. But for the sake of determination *u*-values which are higher than 10 m s^{-1} and *rh*-values which are lower than 25% are supposed to present a reasonable "saltation window" [42,43]. An experimental parameter study dealing with erosion effects on silvered-glass reflectors concluded that 10 m s^{-1} is a reasonable threshold value for *u* when a MIL-dust is used under 45° impact angle [31]. Therefore the respective *u-rh* couples are circumscribed by the red rectangle in Fig. 5 and the comprised absolute hours are given in the upper right part of each figure. They are 118, 34, 211 and 5 h for MIS, ERF, ZAG and PSA, respectively. This finding points to an elevated saltation potential for the MIS and ZAG in comparison to the other two sites, since low relative humidity accompanied by high wind velocities favors the saltation activity [43].

3.1.3. Erosion potential matrix

In order to achieve a more structured assessment of the sandstorm damage potential at unknown sites, the following matrix (see Table 3), which is a qualitative summary of all the earlier investigated site characteristics, can be used. Six of the seven different factors are taken from [12] (leaving apart TSP, since it has not been part of the current work) and were evaluated for the five investigated sites. From the analysis of the soil samples, the meteorological data and the description of the surrounding area of the outdoor sites, the cells of the matrix are filled with red color if the respective factor displays a potential erosion risk and with green color if no erosion risk is present at the respective site. Yellow color is used for intermediate values. Since no *u-rh* evaluation is made for Chajnantor, the respective cell remains white. From this representation it can be seen, that the highest erosion risk is identified in ZAG where all the cells are colored in red. The second position takes on CHA with three red cells and the rest of them in yellow while the *u-rh* cell remains white due to insufficient data. For MIS, ERF and PSA, only two criteria are marked in red and the rest of the cells are colored in yellow or green. Consequently a low erosion risk is assumed for those three sites.

3.1.4. Analysis of outdoor exposed reflectors

In order to accurately assess the potential risk of erosion due to sandstorms and check the validity of the matrix shown in Table 3, exposure of representative material samples is essential. Microscope images of two different magnification levels of the front glass surface of the reflectors, which were exposed at the five sites analyzed, are shown in Fig. 6. It can be seen that after the 12 months exposure in MIS, ERF and PSA, the glass does not exhibit any noticeable defects. Only some adhering particles on the surface can be noticed. Since they were also present in the as-received status of the reflectors, and can hardly be

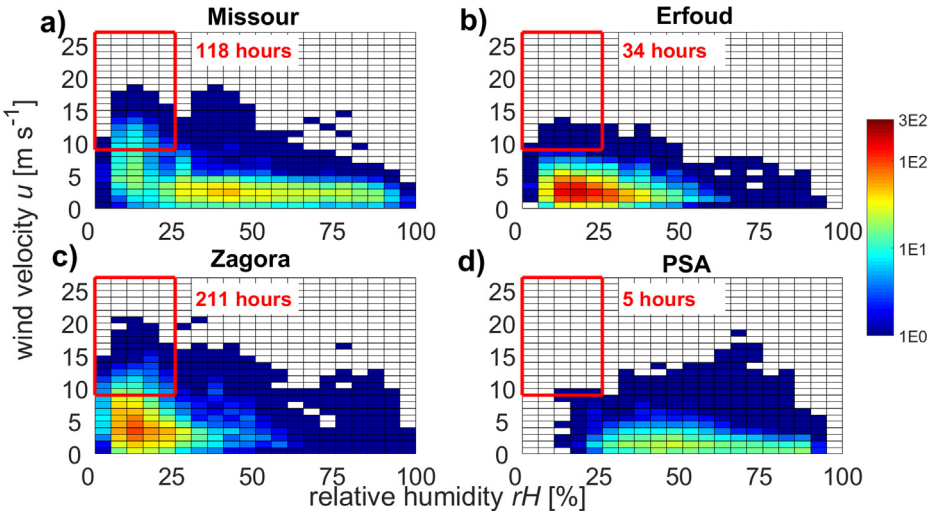

Fig. 5. u-rh couples for MIS, ERF, ZAG and PSA during one meteorological year for winds blowing in south direction (180 ± 90°). Color codes the absolute hours of the respective *u-rh* couples. The red number in the upper right corner corresponds to the hours measured in the red square.

Table 3
Erosion potential matrix for the five investigated sites. Cells are colored from red, over yellow to green, for high, intermediate and low erosion risks of the respective column parameter for each site.

	PSD_{num} maximum at 65-200 µm	PSD_{num} bimodal	Open terrain with u>10 m/s	Low *rh* and high *u* simultaneously present	Low clay content	High quartz content
MIS						
ERF						
ZAG						
PSA						
CHA						

avoided because of the handling in the laboratory, the sample can be regarded as almost indistinguishable from its initial conditions through visual inspection. Contrarily, the reflector which was exposed in ZAG shows clear signs of degradation. A high density of defect spots with typical dimensions of a few µm can be seen. Alongside of the shallow surface scratches, lateral cracks with diameters of around 100 µm and depths of around 50 µm can be noticed as well. The reflector exposed in CHA exhibits those large defects as well, but lacks the high density of small scratches observed in ZAG. Apart from some lateral cracks, the glass surface appears largely unaffected.

The damages caused by environmental conditions at the exposed reflectors can be quantified by measuring $\rho_{\lambda,\varphi}$. The reflectors are measured before and after the 12 months exposure at the respective sites and the $\Delta\rho_{\lambda,\varphi}$ is calculated. The obtained values can be read out from Table 4. After the exposure at MIS, ERF and PSA, $\Delta\rho_{\lambda,\varphi}$ lies in the range of the measurement uncertainty and can therefore be regarded as insignificant. For ZAG and CHA however $\rho_{\lambda,\varphi}$ decreases by 4.5 ± 0.3 ppt and 0.6 ± 0.1 ppt, respectively. Since the hemispherical reflectance of all samples is measured as well and no significant drop can be detected, it can be argued that $\Delta\rho_{\lambda,\varphi}$ is rather the result of increased scattering on the glass surface caused by scratches and cracks than of degradation effects of the silver layer. The surface defects are not only the source of increased light scattering but further present efficient deposition areas for small dust particles and can hence increase the overall soiling effects on the reflector surface.

It shall be pointed to the fact that the determined $\Delta\rho_{\lambda,\varphi}$ values are representing a worst-case scenario, and for several reasons the overall optical performance of solar power plants is not supposed to exhibit the same drastic degradation behavior at the respective sites. It is known from wind tunnel experiments that the transported sand mass depends exponentially on the height above the ground [44], and it can therefore be concluded that the number of defects, caused by saltating sand particles is very sensitive to slight changes of the exposure height. It might well be that the here used exposure height of 1.2 m is representative for the bottom edge of a parabolic trough receiver, but it's unrealistic to assume the same erosion effects over the complete aperture of e.g. 5.7 m for an Euro trough model. Apart from the height dependence, a strong influence of wind blocking obstacles is expected. The outermost structures of a solar plant which are facing the predominant wind direction might experience such strong erosion effects like it was measured in the here performed outdoor study, but inner loops, panels, heliostats etc. are expected to be shielded from the strong erosion by the outer parts of the plant. By the installation of wind fences a shielding effect could also be achieved for the outermost parts of the solar power plant.

From the image analysis procedure which was described in section 2.2, the DSDD was developed for the five sites and is displayed in Fig. 7a. Since MIS, ERF and PSA exhibit very similar results, they were merged into one data series named *erosivity class 1*. For this class, no larger defects than ca. 8 µm are observed and the DSDD evaluation was performed using the 50-fold magnification pictures only. Also the amount of defects detected in each size bin is lowest for class 1 compared to the other two sites and lies at a few thousand defects per cm^2 reflector area. On the reflectors from ZAG and CHA, the complete D_d-spectrum is present. As well as for class 1, the *DD* exhibits the highest values for the smallest size bin (representing defects with $D_d = 1–2\ \mu m$) and decreases exponentially with increasing D_d. The largest defects for both ZAG and CHA are measured to be around 100 µm. For the sake of better visibility, the respective figures are limited to the region from 0 to 50 µm, since larger defects are only very sporadic. It is important to note that the *DD* between 1 and 20 µm is the largest for ZAG and it lies between one and two orders of magnitude above the *DD* of CHA in that particular range.

By having a look at the two different *DD* for the 10 and 50-fold magnification images, it can be seen that *DD* is higher for the 50-fold magnification, in the case of ZAG the factor is around two and in CHA around three. Taking into account the arbitrary selected values for illumination threshold, particle size cut offs and edge effects when changing from one microscope objective to another, this can be regarded as a satisfying result.

In general, the presentation in Fig. 7a quantifies what became obvious from the visual inspection and the microscope pictures. To better understand the relevance of the distinct D_d-bins for $\rho_{\lambda,\varphi}$, the surface coverage of each bin was determined by multiplying the number of the defects with their respective average size and the resulting distribution is displayed in Fig. 7b. Two conclusions can be drawn from this graph: Firstly, surface coverage is largest on the reflectors exposed in ZAG followed by those from CHA and then by the class 1 sites. By integrating this graph, the total surface coverage of all detected defects is determined to be 6.05, 0.45 and 0.06% for the reflectors from ZAG, CHA and the class 1 sites, respectively. In the overlapping range of the 50X and 10X data of ZAG and CHA, the mean value is used. Secondly, it can be concluded that small defects play the major role when the surface coverage is taken into consideration. Therefore, it can be argued that among the evaluated defects, those ones in the smallest D_d-bins between 1 and 10 µm are mainly contributing to $\Delta\rho_{\lambda,\varphi}$.

However, it has to be stated that realistic erosion simulations should reproduce all the defects, including the large defects even though they do not lead to a significant proportion of $\Delta\rho_{\lambda,\varphi}$. The specular reflectance might be the key parameter for quality assessment in the first place, but the consequences of the large defects for further aging mechanisms such as corrosion, thermal fracture, increased soiling, etc. might be harmful in a second step process that could not be detected in the timeframe of 12 months. Further, it might be possible that because of the absence of specific environmental conditions at the respective sites, those second step processes might never be observed in the current study. Further research is needed, that addresses second step aging mechanisms of solar glass exhibiting comparable defect sizes, when exposed to thermal gradient or accelerated soiling tests. Nevertheless, the goal of a successful accelerated aging simulation should be the reproduction of the DSDD, which is detected on the outdoor exposed reflectors. If no further environmental aging effects are responsible for a comparable $\Delta\rho_{\lambda,\varphi}$, the

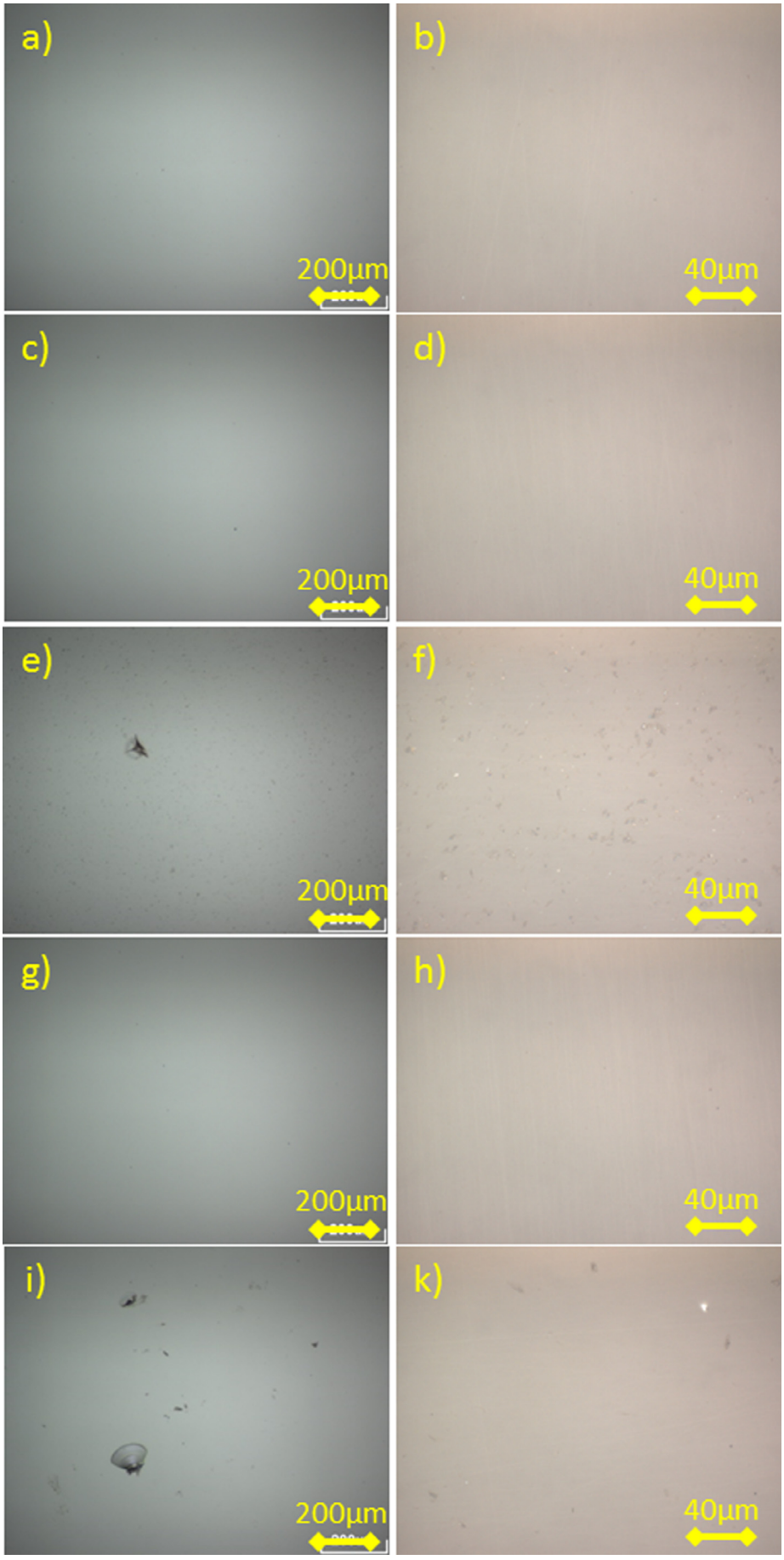

(caption on next page)

Fig. 6. Microscope images with 10 (left column) – and 50-fold (right column) magnification of the glass surface of the reflectors from a, b) MIS, c, d) ERF, e, f) ZAG, g, h) PSA and i, k) CHA.

Table 4
Monochromatic specular reflectance values of solar reflectors in their initial state, after 12 months exposure at five outdoor sites and the respective reflectance drop.

site	$\rho_{\lambda,\varphi}$						$\Delta\rho_{\lambda,\varphi}$		
	initial			12 months					
MIS	0.961	±	0.000	0.961	±	0.001	−0.001	±	0.001
ERF	0.960	±	0.001	0.961	±	0.001	−0.001	±	0.001
ZAG	0.962	±	0.000	0.917	±	0.003	−0.045	±	0.003
PSA	0.964	±	0.001	0.962	±	0.002	−0.002	±	0.002
CHA	0.960	±	0.001	0.954	±	0.001	−0.006	±	0.001

artificial simulation of the measured DSDD in the laboratory will automatically lead to a comparable $\Delta\rho_{\lambda,\varphi}$. Since no corrosion defects were detected on the exposed mirror samples it is highly likely that erosion was the only degradation mechanism responsible for the reflectance loss for the sites studied.

3.1.5. Erosivity class

From the acquired knowledge about the meteorological conditions and surface morphology of the investigated outdoor sites and the corresponding erosion effects on exposed silvered-glass reflectors, erosivity classes are defined (see Table 5). This is done in accordance to corrosivity classes from [45] where a class 1 environment represents a mild environment and class 3 harsh conditions with respect to the environmental effect. It is important to mention that there is a crucial difference in the validity of corrosivity and erosivity classes for a specific site. This follows from the increased dependence of specimen orientation on the observed degradation levels for erosion effects. While it can easily be understood that both the horizontal and the vertical orientation of the specimen do only play a minor role for corrosion effects, this statement does not hold true for erosion which is governed in a principal way by the orientation of the specimen towards the wind direction. Also the height above the ground determines the intensity of the erosion effects considerably. In the current work the erosivity class definition is strictly coupled to the main exposure characteristics: south-orientation (north for CHA), horizontal elevation of 45° and approximate height above ground of (1.2 ± 0.2) m.

3.2. Artificial aging experiments

Once the five studied sites are classified into three erosivity classes, the experiments to simulate the DSDD of the outdoor reflectors in the laboratory are divided accordingly. Initial testing made clear that none of the two selected artificial erosion materials could reproduce all the observed defects on the outdoor exposed reflectors alone. Therefore mixtures of MIL-dust and MIL-sand are produced and after several trials and consecutive linear combinations of the resulting DSDD, adequate compositions are found. To reproduce the annual defects of the class 1 sites, $m_a = 0.006$ g/cm^2 of MIL-dust is used. For the simulation of the effects of class 2, $m_a = 0.016$ g/cm^2 of MIL-dust is mixed with $m_a = 0.073$ g/cm^2 of MIL-sand. For the simulation of the effects of class 3, the composition is 0.764 g/cm^2 and 0.016 g/cm^2 for MIL-dust and MIL-sand, respectively. Fig. 8 depicts the comparison of the resulting DSDD of the artificially aged reflectors with the DSDD which was obtained after the 12 months outdoor exposure as already shown in Fig. 7a, now separated for the different erosion classes.

It can be observed that the erosion simulation based on empirically found m_a quantities, match the DSDD like they are obtained for the outdoor exposed reflectors quite well. Over the complete investigated D_d –range, the density of the artificially provoked defects in the Acetube follows the same trend and always lays in the same order of magnitude as for the respective outdoor sample. The $\rho_{\lambda,\varphi}$ is measured before and after the erosion simulation and the respective values can be read out from Table 6. The measured reflectance drops of -0.001 ± 0.001 and -0.006 ± 0.002 for the class 1 and class 2 samples respectively match exactly the $\Delta\rho_{\lambda,\varphi}$ values obtained for the outdoor exposure (see Table 4). For the class 3 simulation, $\Delta\rho_{\lambda,\varphi}$ from the laboratory experiment exhibits a value which is, with -0.039 ± 0.002, slightly below the $\Delta\rho_{\lambda,\varphi}$ of -0.045 ± 0.004 from the Zagora site. It is noteworthy that the developed procedure to simulate accurate erosion defects on the glass surface, which was purely based on an image processing technique applied to microscope pictures of the glass surface, leads to the coinciding specular reflectance drop values. The remaining discrepancy between the actual and the simulated $\Delta\rho_{\lambda,\varphi}$ for class 3 could be explained by the contribution of defects in the sub micrometer range. Because of the limitations of the here used microscope setup, this instance cannot be verified and would have to be investigated further via higher optical magnifications or electron microscopy.

The similarity of the DSDD is already verified by the graphs in Fig. 8

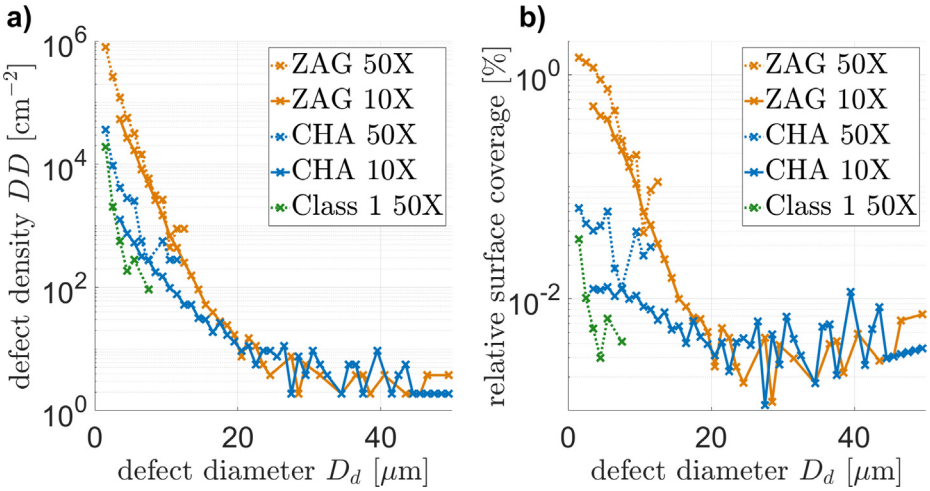

Fig. 7. a) DSDD per square centimeter; b) relative surface coverage. The sites MIS, ERF and PSA were merged to one dataset labeled Class 1. The addition "10X" and "50X" indicates the magnification of the source images.

Table 5
Spatial parameters of the defects and consecutive optical properties of reflectors exposed at sites of the respective erosivity class. Definitions apply for 12 months exposure with 45° horizontal elevation to the South (North for CHA) at (1.2 ± 0.2) m above ground.

Erosivity class	Reference site	Typical monochromatic specular reflectance loss caused by erosion $\Delta\rho_{\lambda,\varphi}$ [-]	Maximum defect size [μm]	Total damaged area due to erosion [%]
1	MIS, ERF, PSA	Negligible (> -0.002)	8	0.06
2	CHA	−0.006	100	0.45
3	ZAG	−0.045	100	6.05

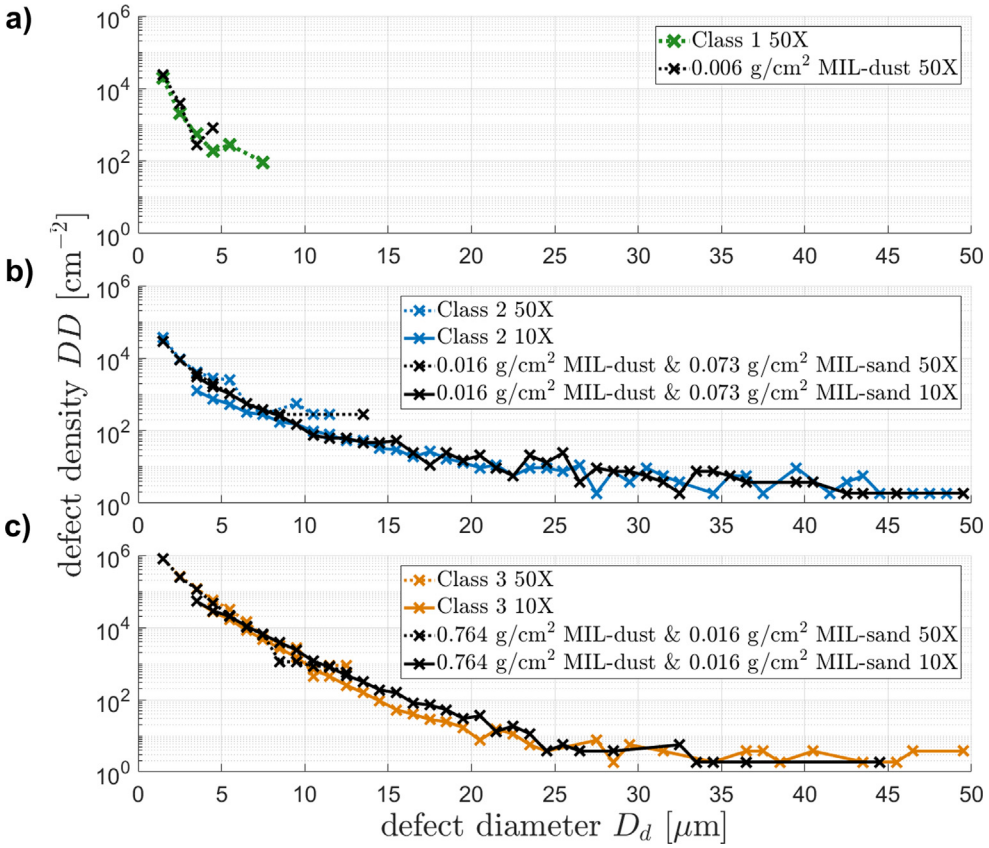

Fig. 8. DSDD per square centimeter of the reflectors exposed outdoor for 12 months (in color) and their respective laboratory simulation (black). The simulation is done for a) class 1 (MIS, ERF, PSA), b) class 2 (CHA) and c) class 3 (ZAG). The addition "10X" and "50X" indicates the magnification of the source images.

and the consecutive reflectance analysis did confirm this instance as well. For the reason of completeness, Fig. 9 shows a microscope comparison of the glass surface of the actual reflector sample that was exposed for 12 months in Zagora and the reflector that was treated in the laboratory erosion simulation, with the respective parameters, developed for the erosivity class 3. By a look at both of the pictures, one can easily realize that the developed erosion procedure provokes the same defects as observed outside very well.

4. Conclusions

In the first part of the here presented work a detailed look on five potential solar power sites regarding their sandstorm occurrence risk is taken. Six key aspects dealing with the meteorological conditions, the topography and the soil characteristics were analyzed. The resulting data is introduced in an erosion potential matrix and its correct applicability could be verified by the analysis of state of the art solar reflectors, which were exposed at the respective sites for 12 months. The site, which displayed the most dangerous situation for frequent sandstorm events was found to be Zagora, and indeed did the reflector from that site exhibit the strongest optical performance loss. Therefore it can be concluded that the elaborated erosion matrix is suitable to quickly assess an unknown site regarding its potential danger for sandstorm occurrence.

Table 6
Specular reflectance values of artificially eroded reflectors and the employed m_a values which are used in order to reproduce the effects of the respective erosivity classes.

erosivity class	m_a MIL-dust [g/cm²]	m_a MIL-sand [g/cm²]	Initial $\rho_{\lambda,\varphi}$ [-]	final $\rho_{\lambda,\varphi}$ [-]	$\Delta\rho_{\lambda,\varphi}$ [-]
1	0.006	–	−0.964 ± 0.001	−0.963 ± 0.001	**−0.001 ± 0.001**
2	0.016	0.073	−0.964 ± 0.001	−0.959 ± 0.001	**−0.006 ± 0.001**
3	0.764	0.016	−0.964 ± 0.000	−0.925 ± 0.002	**−0.039 ± 0.002**

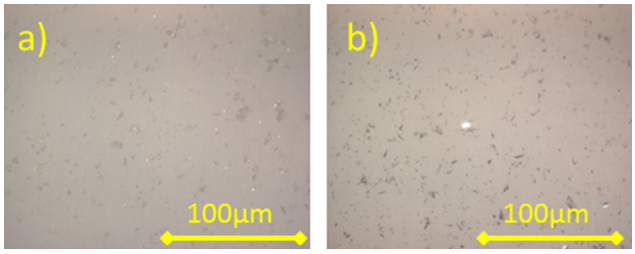

Fig. 9. Microscope images (50x) of glass reflector surface after a) 12 month exposure to Zagora and b) after laboratory erosion simulation (erosivity class 3).

The five reflector samples which were exposed outdoor were analyzed in the laboratory via a novel image processing technique, which is able to determine the defect density size distribution (DSDD) present on the glass surface of the reflector. By the application of this method, three erosivity classes are attributed to the outdoor exposure sites in dependence on the erosion severeness. Afterwards, the input parameters of a specially developed laboratory erosion setup are tuned in such a way, that the resulting DSDD matches the one from the outdoor exposure. The successful simulation of the outdoor behavior is verified by optical reflectance measurements for all three erosivity classes. The major benefit of this work is that the herein developed method of accelerated erosion testing is also applicable to other material samples, enabling to rapidly predict their performance at outdoor exposure sites of erosivity class 1–3.

CRediT authorship contribution statement

F. Wiesinger: Conceptualization, Methodology, Software, Validation, Investigation, Writing - original draft, Writing - review & editing. **F. Sutter:** Funding acquisition, Project administration, Writing - review & editing. **A. Fernández-García:** Project administration, Writing - review & editing. **J. Wette:** Writing - review & editing. **N. Hanrieder:** Investigation. **F. Wolfertstetter:** Investigation. **Martin Schmücker:** Supervision. **R. Pitz-Paal:** Supervision.

Declaration of Competing Interest

The authors declare that they have no known competing financial interests or personal relationships that could have appeared to influence the work reported in this paper.

Acknowledgments

The research conducting to the results of this paper were funded by the EU H2020 project RAISELIFE under Grant Agreement 686008.

References

[1] Márquez FPG, Karyotakis A, Papaelias M. Renewable energies: Business outlook 2050. Springer; 2018.
[2] Ruiz-Arias JA, Gueymard CA, Santos-Alamillos FJ, Pozo-Vázquez D. Worldwide impact of aerosol's time scale on the predicted long-term concentrating solar power potential. Sci Rep 2016;6:30546.
[3] Sarver T, Al-Qaraghuli A, Kazmerski LL. A comprehensive review of the impact of dust on the use of solar energy: history, investigations, results, literature, and mitigation approaches. Renew Sustain Energy Rev 2013;22:698–733.
[4] F. Wolfertstetter, Effects of Soiling on Concentrating Solar Power Plants, in, 2016.
[5] N. Hanrieder, Determination of Atmospheric Extinction for Solar Tower Plants, in, 2016.
[6] Gonzalo AP, Marugán AP, Márquez FPG. A review of the application performances of concentrated solar power systems. Appl Energy 2019;255:113893.
[7] Maghami MR, Hizam H, Gomes C, Radzi MA, Rezadad MI, Hajighorbani S. Power loss due to soiling on solar panel: a review. Renew Sustain Energy Rev 2016;59:1307–16.
[8] Bouaddi S, Fernández-García A, Sansom C, Sarasua J, Wolfertstetter F, Bouzekri H, et al. A review of conventional and innovative-sustainable methods for cleaning reflectors in concentrating solar power plants. Sustainability 2018;10:3937.
[9] Hanrieder N, Wilbert S, Mancera-Guevara D, Buck R, Giuliano S, Pitz-Paal R. Atmospheric extinction in solar tower plants–A review. Sol Energy 2017;152:193–207.
[10] Hanrieder N, Sengupta M, Xie Y, Wilbert S, Pitz-Paal R. Modeling beam attenuation in solar tower plants using common DNI measurements. Sol Energy 2016;129:244–55.
[11] Hanrieder N, Ghennioui A, Alami Merrouni A, Wilbert S, Wiesinger F, Sengupta M, et al. Atmospheric Transmittance Model Validation for CSP Tower Plants. Remote Sensing 2019;11:1083.
[12] Wiesinger F, Sutter F, Wolfertstetter F, Hanrieder N, Fernández-García A, Pitz-Paal R, et al. Assessment of the erosion risk of sandstorms on solar energy technology at two sites in Morocco. Sol Energy 2018;162:217–28.
[13] Schiller M, Höing T. Leistungsfähige Spiegel für solarthermische Kraftwerke (high performance reflectors for CSP plants). Vak Forsch Prax 2012;24:14–7.
[14] Fernández-García A, Cantos-Soto ME, Röger M, Wieckert C, Hutter C, Martínez-Arcos L. Durability of solar reflector materials for secondary concentrators used in CSP systems. Sol Energy Mater Sol Cells 2014;130:51–63.
[15] Sansom C, Comley P, King P, Almond H, Atkinson C, Endaya E. Predicting the Effects of Sand Erosion on Collector Surfaces in CSP Plants. Energy Procedia 2015;69:198–207.
[16] Karim M, Naamane S, Delord C, Bennouna A. Laboratory simulation of the surface erosion of solar glass mirrors. Sol Energy 2015;118:520–32.
[17] Humood M, Beheshti A, Meyer J, Polycarpou AA. Normal impact of sand particles with solar panel glass surfaces. Tribol Int 2016;102:237–48.
[18] A. Matal, S. Naamane, H. Bouaouinel, Laboratory Erosion Simulation of Antisoiling Glass Mirror. 2018 6th International Renewable and Sustainable Energy Conference (IRSEC); 2019 IEEE.
[19] Völker C, Philipp D, Masche M, Kaltenbach T. Development of a test method for the investigation of the abrasive effect of sand particles on components of solar energy systems. Proceedings of the European PV Solar Energy Conference. Amsterdam 2014.
[20] Wiesinger F, Sutter F, Fernández-García A, Reinhold J, Pitz-Paal R. Sand erosion on solar reflectors: accelerated simulation and comparison with field data. Sol Energy Mater Sol Cells 2016;145:303–13.
[21] Wiesinger F, San Vicente G, Fernández-García A, Sutter F, Morales A, Pitz-Paal R. Sandstorm erosion testing of anti-reflective glass coatings for solar energy applications. Sol Energy Mater Sol Cells 2018;179:10–6.
[22] Datsiou KC, Overend M. Artificial ageing of glass with sand abrasion. Constr Build Mater 2017;142:536–51.
[23] Miller DC, Muller MT, Simpson LJ. Review of Artificial Abrasion Test Methods for PV Module Technology. Contract 2016.
[24] Pescheux A-C, Le Baron E, Raccurt O. Characterization of different Moroccan sands to explain their potential negative impacts on CSP solar mirrors. Sol Energy 2019;194:959–68.
[25] Schüler D, Wilbert S, Geuder N, Affolter R, Wolfertstetter F, Prahl C, et al. The enerMENA meteorological network – Solar radiation measurements in the MENA region. AIP Conf Proc 2016;1734:150008.
[26] enerMENA. https://www.dlr.de/sf/de/desktopdefault.aspx/tabid-8680/12865_read-32404/. (Accessed: 2020-03-05).
[27] Gschwind B, Ménard L, Albuisson M, Wald L. Converting a successful research project into a sustainable service: the case of the SoDa Web service. Environ Modell Software 2006;21:1555–61.
[28] Parameters and Method to Evaluate the Reflectance Properties of Reflector Materials for Concentrating Solar Power Technology Technology, S.R. Guideline, March 2018.
[29] S. Reichenspurner, Particle Erosion on Solar Mirrors: Construction and First Experimental Stage of an Open Loop Wind Tunnel, in, Hochschule Kempten, 2016.
[30] DIN 52348, Prüfung von Glas und Kunststoff, in: Verschleißprüfung - Sandrieselverfahren, Deutsches Institut für Normung, 1985.
[31] F. Wiesinger, Erosion of solar reflectors in desert environments, Ph.D. Thesis, in: Rheinisch-Westfälische Technische Hochschule Aachen, 2018.
[32] Stachowiak G, Batchelor AW. Engineering tribology. Butterworth-Heinemann; 2013.
[33] Wensink H, Elwenspoek MC. A closer look at the ductile–brittle transition in solid particle erosion. Wear 2002;253:1035–43.
[34] Caron S. Accelerated aging of thick glass second surface silvered reflectors under sandstorm conditions, Master level thesis from. European Solar Engineering School, No.146 2011.
[35] Bouaouadja N, Bouzid S, Hamidouche M, Bousbaa C, Madjoubi M. Effects of sandblasting on the efficiencies of solar panels. Appl Energy 2000;65:99–105.
[36] Darmenova K, Sokolik IN, Shao Y, Marticorena B, Bergametti G. Development of a physically based dust emission module within the Weather Research and Forecasting (WRF) model: assessment of dust emission parameterizations and input parameters for source regions in Central and East Asia. Journal of Geophysical Research: Atmospheres 2009;114.
[37] Bagnold RA. The Physics of Blown Sand and Desert Dunes. New York: William Morrow and Company; 1954.
[38] R. Greeley, J.D. Iversen, Wind as a geological process: on Earth, Mars, Venus and Titan, CUP Archive, 1987.
[39] Mikami M, Yamada Y, Ishizuka M, Ishimaru T, Gao W, Zeng F. Measurement of saltation process over gobi and sand dunes in the Taklimakan desert, China, with newly developed sand particle counter. Journal of Geophysical Research: Atmospheres 2005;1984–2012:110.
[40] Fécan F, Marticorena B, Bergametti G. Parametrization of the increase of the aeolian erosion threshold wind friction velocity due to soil moisture for arid and semi-arid

areas. Ann Geophys 1998;17:149–57.
[41] Ravi S, D'Odorico P. A field-scale analysis of the dependence of wind erosion threshold velocity on air humidity. Geophys Res Lett 2005;32.
[42] Boddupalli N, Singh G, Chandra L, Bandyopadhyay B. Dealing with dust – Some challenges and solutions for enabling solar energy in desert regions. Sol Energy 2017;150:166–76.
[43] Yang X, He Q, Mamtimin A, Huo W, Liu X. Diurnal variations of saltation activity at Tazhong: the hinterland of Taklimakan Desert. Meteorol Atmos Phys 2013;119:177–85.
[44] Williams G. some aspects of the aeolian saltation load. Sedimentology 1964;3:257–87.
[45] ISO 9223, Corrosion of metals and alloys - Corrosivity of atmospheres - Classification, determination and estimation, International Organization for Standardization, 2012.